Available online at www.sciencedirect.com
ScienceDirect
Journal of Molecular Catalysis A: Chemical 272 (2007) 118–127
JOURNAL OF MOLECULAR CATALYSIS A: CHEMICAL
www.elsevier.com/locate/molcata

Modeling of surface explosion of NO + H_2 reaction on Pt(1 0 0): Mean-field analysis and dynamic Monte Carlo simulations

Luis Vicente [a,*], Francisco Vidal Caballero [b]

[a] *Departamento de Física y Química Teórica, Facultad de Química, UNAM, 04510 Mexico, D.F., Mexico*
[b] *Tecnológico de Estudios Superiores de Ecatepec, Av. Hank González s/n, Col. Valle de Anáhuac, Ecatepec de Morelos, 55210 Estado de México, Mexico*

Received 28 November 2006; received in revised form 8 March 2007; accepted 9 March 2007
Available online 19 March 2007

Abstract

Surface explosions which occur, for example, in field ion microscopy experiments on catalytic reduction of nitric oxide by H_2 over Pt surfaces are studied as a function of partial pressures and initial species covering. Using a Langmuir-Hinshelwood mechanism of reaction a simplified model with only four adsorbed species NO,H,O,N is constructed. This minimal model, in the mean field approximation (MF), shows a bistability, which is associated to the explosive phenomena. Near the transition point between these states there exist a peak in the production rates which is associated to an abrupt growing of the empty sites, far from the transition point the production rates only attains a stationary value. Dynamic Monte Carlo simulations were performed and compared with the MF results. Dynamic Monte Carlo simulations allow to study the spatial development of explosions. It is shown that at the peak of the production rates there is an island formation of adsorbed NO surrounded by empty sites which provokes the rapid decomposition of NO into adsorbed N and O and, consequently, a large production of N_2 and H_2O.

Keywords: Desorption; Kinetics; Dynamic Monte Carlo; NO reduction; Modelling

1. Introduction

The catalytic reaction of NO over noble metals with CO or H_2 has been the subject of many studies because it is an important reaction in automotive catalyst used for air pollution control [1].

The major reactions of NO conversion to nitrogen in the automotive catalytic converter are (Taylor [1]; Egelhoff [2]):

$$2NO + 2H_2 \rightharpoonup N_2 + 2H_2O$$

$$2NO + 2CO \rightharpoonup N_2 + 2CO_2$$

however, this last step is too slow to provide a major path for NO reduction [2] and NO can also react to produce NH_3:

$$NO + \frac{5}{2}H_2 \rightharpoonup NH_3 + H_2O$$

The temperature and the feed composition govern the selectivity of this reaction.

Surface chemical reactions have a central role in the processes of heterogeneous catalysts. In a catalytic process, the molecules of reactants are adsorbed from the gas phase onto a metal surface, diffuse on it and react to form a product that goes back to the gas phase. Under specific values of the system parameters, as partial pressures, these reactions can exhibit complex dynamical behaviour as oscillations, pattern formation and chaotic behaviour. Oscillations will not occur if the deviations from equilibrium are small and in this case linear relations can describe the system. The oscillations occur due to feedback, either chemical (such as autocatalysis) or due to temperature (as in a non-isothermal reaction). Heterogeneous catalytic reactions satisfy the necessary requirements for the appearance of auto-oscillations because the continuous mass flow of reactants and heat exchange with the surroundings. The flux of energy and matter through the open system maintain it far from equilibrium and temporal and spatial organization become possible.

Kinetic oscillations for the reaction NO + H_2 over Pt single crystals were found to occur for gas reactant pressures in the

* Corresponding author. Tel.: +52 55 56223803; fax: +52 55 6223719.
E-mail address: luis.vicente@servidor.unam.mx (L. Vicente).

1381-1169/$ – see front matter © 2007 Elsevier B.V. All rights reserved.
doi:10.1016/j.molcata.2007.03.035

Nomenclature

k_i	reaction rates
L	characteristic length of catalyst
p_{NO} NO	partial pressure (mbar)
$p_{H_2}H_2$	partial pressure (mbar)
R_i	rates of elementary reaction steps
$R_p = \frac{p_{H_2}}{p_{NO}}$	relation of partial pressures
S_i	sticking probabilities, i = NO,H_2
t	time (s)
T	catalyst temperature (K)

Greek letters

θ_i	fractional coverage of chemisorbed species, i = NO,H,N,O
θ_*	fraction of free adsorption sites

range 10^{-6} to 10^{-5} mbar and in the range of temperatures from 430 to 500 K [2–8]. To describe the occurrence of kinetic oscillations, Cobden et al. [9] have proposed a "vacancy" mechanism. In this "vacancy model", the oscillations are due to autocatalytic surface reaction, which increase the number of vacant sites for NO dissociation. Later, Makeev and Niewenhuys [4] have developed a mathematical model to prove that autocatalysis of NO decomposition by vacant sites is one of the main properties that keeps the system oscillating. A very important ingredient of this model is the coverage dependency of the activation energies for NO and CO desorption. So, in this model the system presents oscillatory behaviour without involvement of the surface structural transformation, hex $\rightharpoonup$ 1 × 1, which takes place on Pt surfaces due to the presence of adsorbents. This later mechanism has been shown to be important for other chemical oscillations such as those in NO + CO. Theoretical models for the NO + H_2 reaction which takes this effect into account are found, for example, in refs. [10,11]. Reviews of these oscillating reactions and others are found in refs. [12,13].

Another important property of the above mentioned reaction is the so-called "surface explosion", where the coadsorbed NO and H_2 react abruptly to form extremely narrow product peaks observed in temperature-programmed reaction experiments [14]. This sudden increase in the reaction products N_2 and H_2O, has also been observed in field ion microscopy experiments (FIM) and field electron microscopy (FEM) of the NO + H_2 reaction on a Pt emitter tip [15–17]. In this case, the microscope is run as a flow reactor with a constant flux of reactant and fixed temperature.

Traditionally, the description of such process has been via the mean field (MF) approach in the reaction kinetics, that is, through ordinary differential equations (ODE). It leads to a comprehension of non-linear phenomena through linear stability and bifurcation analysis. Such type of approach naturally involves a coarse grained description, and spatial fluctuations that lie below the typical length scale of the coarse graining (about 1 nm) are entirely neglected. Although such a description is sufficient to describe kinetic oscillations, the description of more complex dynamical phenomena, such as, for example, pattern formation, necessarily involves the addition of ad hoc terms in the equations. Some of these limitations can be partially overcome by the use of computer simulations (Monte Carlo, Cellular Automata) where local environments are explicitly taken into account and incorporate the discreteness of reactive events. Although, this type of description still involves some coarse graining at the level of the microscopic description, it has been argued that the associated typical length scales are smaller (about 10–100 μm), and allows the description of pattern formations without extra hypothesis on the kinetic of the reactions themselves. The first of these MC simulations has been the pioneering work of Ziff et al. [18] for a model of CO oxidation on metal surfaces. A review in this field can be found in refs. [19,20].

In a stochastic simulation the dynamic is determined by a master equation

$$\frac{\partial P_\alpha}{\partial t} = \sum_\beta (W_{\beta\to\alpha} P_\beta - W_{\alpha\to\beta} P_\alpha)$$

where P_α and P_β are the probabilities to find the system in the configurations α and β, respectively. $W_{\beta\to\alpha}$ are the transition probabilities per unit time for the different process (adsorption, desorption, etc.). Unfortunately, it is not possible to obtain exact solutions of this equation as one faces an infinite hierarchy of coupled equations for the different probability moments. However, the rates can be related to the experiments, for example, through an Arrhenius-like expression and the steady states are directly related to mean field formulation of the rate evolution equations. Still, as has been discussed by Nicolis [21] a full understanding of the differences between MC results and associated MF description is generally lacking. The simulations nicely complements mean field type approach by allowing the study of the fluctuations of the surface coverage.

The purpose of this paper is to study by dynamic Monte Carlo (DMC) simulations, first the abrupt production of nitrogen and water on a single monolayer of adsorbed NO + H on Pt surfaces, and secondly, we study the rapid catalytic ignition observed in FIM experiments, in both cases, the temperature is maintained fixed. In each case, we compared our results with those obtained by modelling the system through MF kinetic equations.

2. Model

2.1. kinetic equations

We will neglect the relatively poor production of NH_x and N_2O compounds and consider that the reaction proceeds according to the following Langmuir-Hinshelwood mechanism:

$$NO(g) + * \underset{k_3}{\overset{k_1}{\rightleftharpoons}} NO_{ads} \qquad \text{(R1, R3)}$$

$$H_2(g) + 2* \underset{k_4}{\overset{k_2}{\rightleftharpoons}} 2H_{ads} \qquad \text{(R2, R4)}$$

$$2N_{ads} \xrightarrow{k_5} N_2(g) + 2* \qquad \text{(R5)}$$

$$NO_{ads} + * \underset{k_7}{\overset{k_6}{\rightleftharpoons}} N_{ads} + O_{ads} \quad \text{(R6, R7)}$$

$$O_{ads} + H_{ads} \xrightarrow{k_8} OH_{ads} + * \quad \text{(R8)}$$

$$OH_{ads} + H_{ads} \xrightarrow{k_9} H_2O_{ads} + * \quad \text{(R9)}$$

$$H_2O_{ads} \xrightarrow{k_{10}} H_2O(g) + * \quad \text{(R10)}$$

where * denotes a free adsorption site of the Pt(1 0 0)-(1 × 1) surface; NO(g), H_2(g) are the reactants in the gas-phase with partial pressures p_{NO} and p_{H_2}, respectively. The reaction products are N_2(g) and H_2O(g). The adsorbed species are denoted by $(NO)_{ads}$, $(H)_{ads}$, $(N)_{ads}$, $(O)_{ads}$. In the last equations, $R1$ and $R3$ account for NO adsorption and desorption, $R2$ and $R4$ for H_2 adsorption and H desorption, respectively, $R5$ for N desorption, $R6$ for NO dissociation, $R7$ for recombination into NO_{ads}, $R8$ for OH_{ads} formation and $R9$ for H_2O_{ads} formation and $R10$ for H_2O desorption.

The desorption of $(H_2O)_{ads}$ and the hydrogenation of intermediate $(OH)_{ads}$ are assumed to be fast processes. In consequence, only four species are considered (in the following equations the surface coverage are denoted by θ_p, p = NO,H,N,O).

The following coupled ordinary differential equations (ODE's) describe the kinetics of the reaction:

$$\frac{d\theta_{NO}(t)}{dt} = R_1 - R_3 - R_6 + R_7 \quad (7)$$

$$\frac{d\theta_{H}(t)}{dt} = 2R_2 - 2R_4 - 2R_8 \quad (8)$$

$$\frac{d\theta_{N}(t)}{dt} = R_6 - 2R_5 - R_7 \quad (9)$$

$$\frac{d\theta_{O}(t)}{dt} = R_6 - R_7 - R_8 \quad (10)$$

R_i are the rate of the elementary steps ($R1$–$R10$) given above:

$$R_1 = k_1 p_{NO} S_{NO} \theta_*,\ R_3 = k_3 \theta_{NO}$$

$$R_2 = k_2 p_{H_2} S_{H_2} (\theta_*)^2,\ R_4 = k_4 (\theta_H)^2$$

$$R_5 = k_5 (\theta_N)^2,\ R_6 = k_6 \theta_{NO} \theta_*$$

$$R_7 = k_7 \theta_N \theta_O,\ R_8 = k_8 \theta_O \theta_H$$

where $\theta_* = 1 - \theta_{NO} - \theta_H - \theta_N - \theta_O$; $k_\alpha = \nu_\alpha \exp\left[-E_\alpha/RT\right]$, $\alpha = 1, \ldots, 10$; θ_* is a fraction of empty sites available for adsorption, S_i is a sticking coefficient.

The kinetic parameters used in this work are given in Table 1 and were taken from ref. [4].

Table 1
The energy and bare frequency parameters that enter the expression for the various rate constants $k = \nu \exp(-E/RT)$

Reaction step, α	$\nu_\alpha(s^{-1})$	E_α(kcal/mol)
1	2.14×10^5 mbar^{-1}	0
2	8.28×10^5 mbar^{-1}	0
3	1.7×10^{15} mbar^{-1}	37
4	10^{12}	25
5	10^{13}	24
6	2×10^{15}	28
7	2×10^{15}	23
8	10^{13}	13

$S_{NO}k_1 = 1.93 \times 10^5$ (mbar^{-1} s^{-1}), $S_{H_2}k_3 = 1.656 \times 10^5$ (mbar^{-1} s^{-1}).

2.2. Monte Carlo simulations

Dynamic Monte Carlo simulations, from which the behaviour of the catalytic system can be simulated in real time units, were used in the calculations. The algorithm used in this work can be summarized as follows.

The surface of the catalyst is considered to be a two-dimensional lattice of active sites. The surface contains $L^2 = 300 \times 300$ sites with periodic boundary conditions, each site surrounded by eight adjacent sites (this is the so-called Moore neighbourhood consisting of the eight nearest and next-nearest neighbours). On this lattice, the nodes can have the following values: 0 (empty site), 1 (site occupied by NO), 2 (site occupied by H), 3 (site with adsorbed oxygen) or 4 (site occupied by N). Adsorbed species at node r can react with particles on neighbouring sites $r \in N(r)$, with $N(r)$, the Moore neighbourhood defined above. We only consider diffusion of NO, since atomic oxygen is rather immobile on Pt surfaces below $T = 600$ K and the other species have low mobility. Diffusion occurs through random jumps of the adsorbed NO species at node r to one of the empty nodes in the neighbourhood. The rate is typically an order of magnitude larger than the other rates associated with the reaction process.

All of the steps (R1–R8) are taken into account in the MC simulation. The desorption of H_2O is considered to take place immediately after R9.

The numerical implementation of these reactions is essentially similarly to that presented in earlier works [23,24] for the CO + O_2 system.

In this way, we have now 10 possible processes and the set of rate constants is denoted by $K_i (i = 1, \ldots, 10)$. In particular, we will denote by K_H and K_{NO}, the adsorption constants for H and NO, respectively. The rates of NO and H_2 adsorption are considered to be proportional to p_{NO} and p_{H_2}, respectively. The set of reaction rates defines the probability $p_i = K_i / \sum K_i$, that the i-th process is carried out at a lattice point. In our simple scheme, K_i does not depend specifically of the neighbors, for example, the dissociation of NO is independent of the presence of next-neighbor coa-adsorbed N atoms. But, as it will be shown below, with this simple prescription used usually by many authors, the main features of the surface explosion are displayed.

The simulation consists of the following operations:

1. A node r is chosen at random.
2. A process i is chosen with probability p_i.
3. In the case of processes involving simultaneously two adjacent nodes (hydrogen adsorption/desorption, chemical reaction, diffusion), a second node is randomly selected from $N(r)$.

4. If the chosen process is sterically possible in the selected site, it is carried out and values of the sites are updated. If it is not possible, the trial is disregarded. In any case, the sequence is started over from step 1 above.

In DMD, the time is increased by Δt according to

$$\Delta t = -\frac{\ln \xi}{L^2 R}$$

where ξ is a random number selected according to a uniform probability in the interval (0, 1) and R is the sum of all the possible transitions, i.e., the total transition rate of the system. The last relationship establishes the relation between the "arbitrary MC time" and the real time of the system.

At every time, the local occupation numbers characterizes each site

$$n_{i,j}^{\mathrm{NO}}, n_{i,j}^{\mathrm{H}}, n_{i,j}^{\mathrm{O}}, n_{i,j}^{\mathrm{N}}$$

where i, j are the lattice discrete coordinates. The global coverages are then given by:

$$\theta_p = \frac{1}{L}\sum_{i,j} n_{i,j}^{p}$$

with $p = \mathrm{NO,H,O,N,}*$. Besides, the conservation law,

$$\theta_{\mathrm{NO}} + \theta_{\mathrm{H}} + \theta_{\mathrm{O}} + \theta_{\mathrm{N}} + \theta_{*} = 1$$

is maintained.

3. Results

3.1. Reaction and desorption from a monolayer

We consider first the situation, where a NO + H monolayer is already absorbed and analyse the evolution of such monolayer due to the desorption and reaction between species at a given temperature. Steps $R3$–$R10$ proceed: $\mathrm{NO_{ads}}$ can desorbs or dissociate into N and O according to step $R6$; two $\mathrm{N_{ads}}$ can associate into $\mathrm{N_2}$ to desorb as $\mathrm{N_2(g)}$, etc. We have solved Eqs. (1)–(4) for initial conditions $T = 430\,\mathrm{K}$, $\theta_{\mathrm{NO}} = 0.5$, $\theta_{\mathrm{H}} = 0.5$, that is a full monolayer with equal amounts of $\mathrm{NO_{ads}}$ and $\mathrm{H_{ads}}$. The evolution of the adsorbed species is shown in Fig. 1 a. As can be seen, the system attains a final state where it remains only adsorbed oxygen. In Fig. 1 b is shown the evolution in the production of $\mathrm{N_2}$ and $\mathrm{H_2O}$, and as can be seen the rates grow from an initial zero value until they reach a maximum value and then decreases until the rate is null again. The peaks for $r_{\mathrm{N_2}}$ and $\mathrm{H_2O}$ occurs in a very short interval, that is, there is an abrupt or "explosive" production of nitrogen and water. The correlation between the adsorbed species and the rates of production can be inferred from these figures. At first, there is a decrease in $\mathrm{NO_{ads}}$ which dissociates into N and O and these oxygen atoms begin to react with the adsorbed hydrogen until a maximum of water production is attained, this is located around $t \sim 10\,\mathrm{s}$, when θ_{H} is almost half of its initial value. But at $t \sim 20\,\mathrm{s}$, the adsorbed H has already vanished and then the production of water is almost

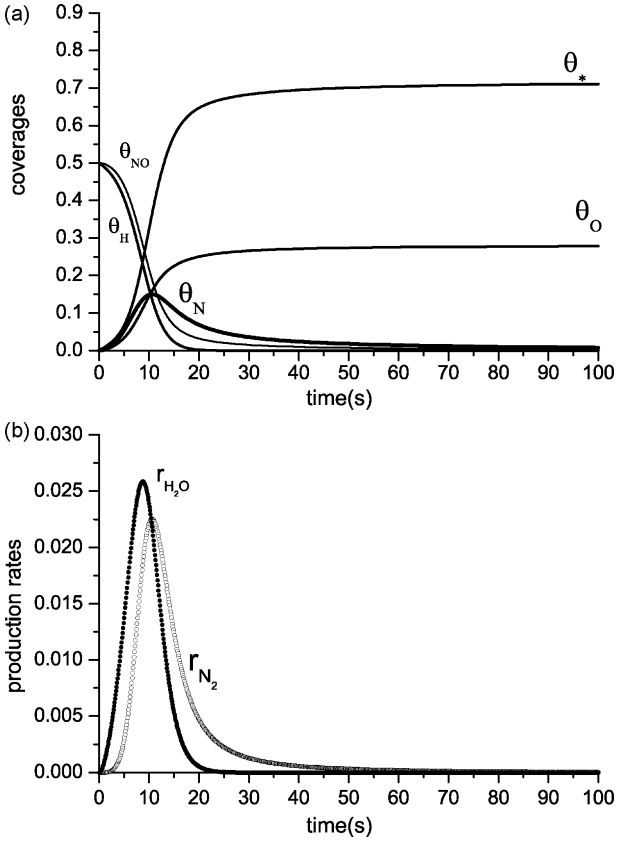

Fig. 1. Mean field description. (a) Adsorbed species vs. time (s) for a $NO + H$ monolayer; (b) the production rates of water, $r_{\mathrm{H_2O}}$ and nitrogen, $r_{\mathrm{N_2}}$. Conditions are $T = 434\,\mathrm{K}$, $p_{\mathrm{NO}} = 1.1 \times 10^{-6}$ mbar and $p_{\mathrm{H_2}} = 7.6 \times 10^{-6}$ mbar.

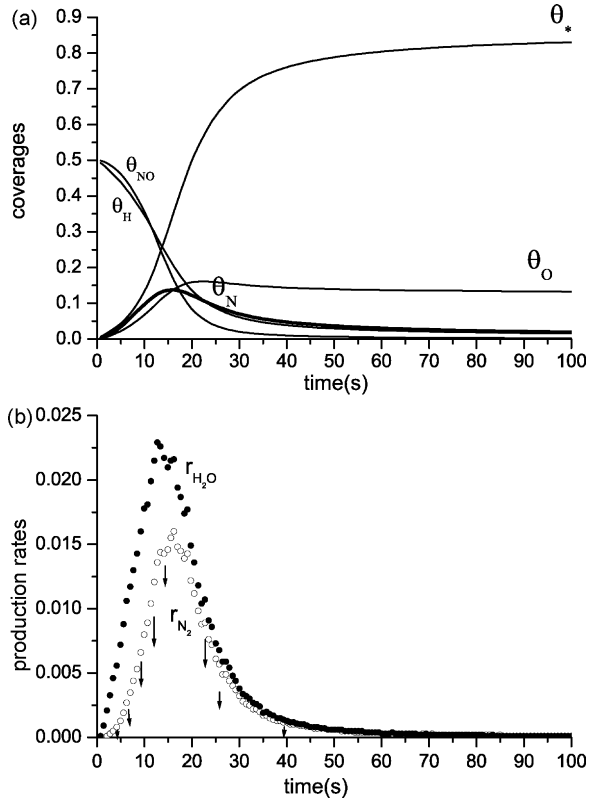

Fig. 2. DMC simulations. (a) Adsorbed species vs. time for a NO + H monolayer; (b) the production rates $r_{\mathrm{H_2O}}$ and $r_{\mathrm{N_2}}$ vs. time averaged over 100 trials.

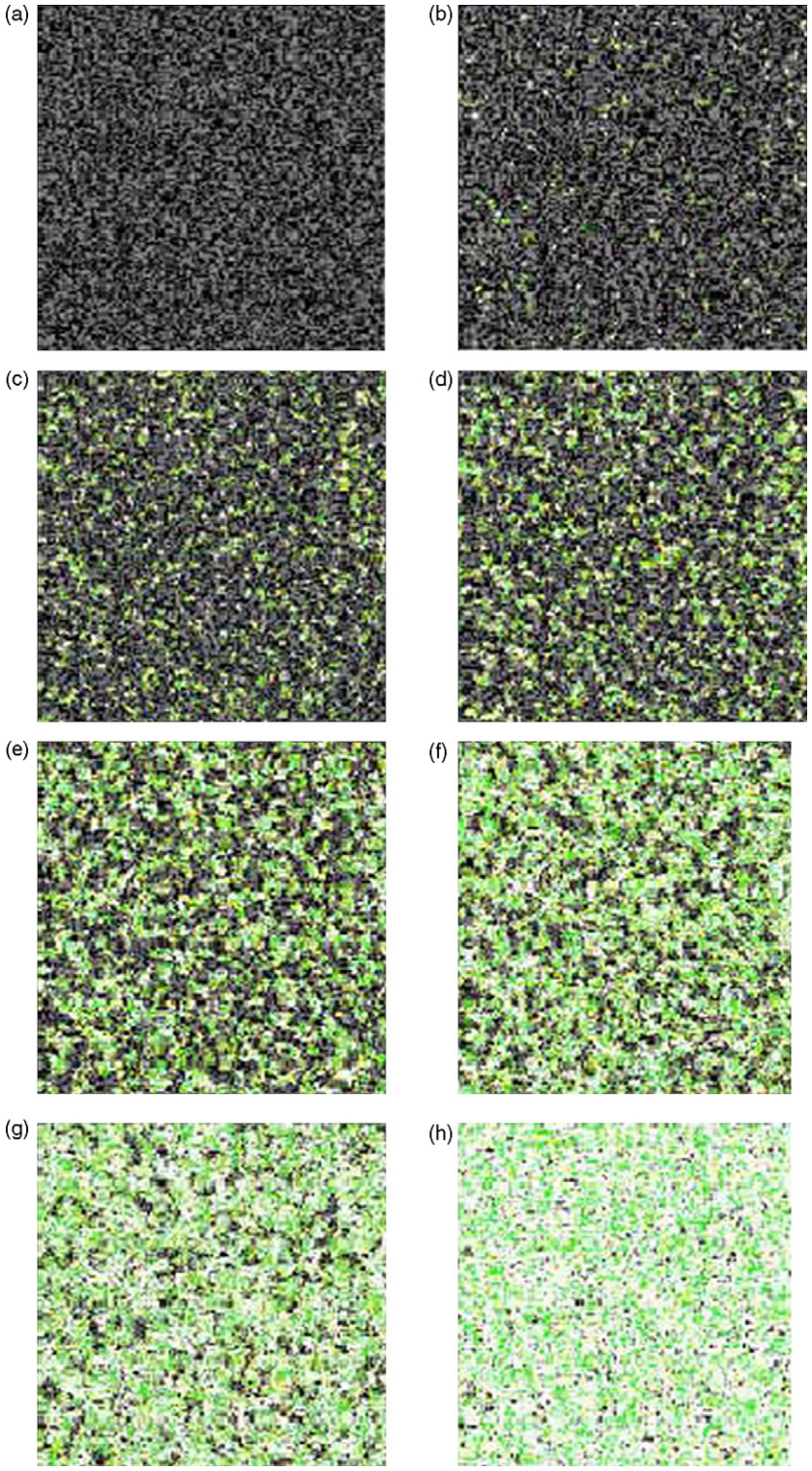

Fig. 3. (a–h) The temporal evolution of the species corresponding to the time series shown in Fig. 2. The time increments correspond to the arrows in the rate evolution shown in Fig. 2, $t \sim 0$, 3, 7, 10, 12, 14, 21, 39 s, respectively. In these images, the grey dots represent adsorbed NO, black dots are adsorbed H, the green dots are adsorbed O, yellow is for adsorbed N and the white sites represent the empty sites. (For interpretation of the references to colour in this figure legend, the reader is referred to the web version of the article.)

zero. The peak of production of N_2 occurs at $t \sim 12$ s which corresponds well with the peak in N_{ads} (Fig. 1a). As time goes on the nitrogen is desorbed and only remains the oxygen on the surface.

Large amounts of DMC calculations were performed to simulate the same situation and conditions stated before. Fig. 2 a and b show the result of our simulations and, as can be see, DMC reproduces well the behaviour as given by the ODE's. Note that

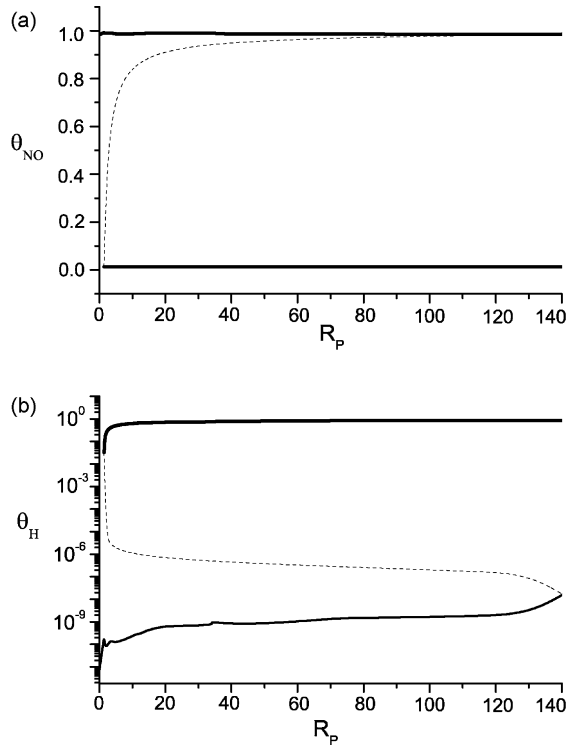

Fig. 4. Calculated steady-states for the control parameter R_p. Here, $T = 434$ K, $p_{NO} = 1.1 \times 10^{-6}$ mbar and p_{H_2} is varied. Steady state (a) NO_{ads} and (b) H_{ads} (logarithmic scale). Stable (unstable) states are shown by solid (dash)lines.

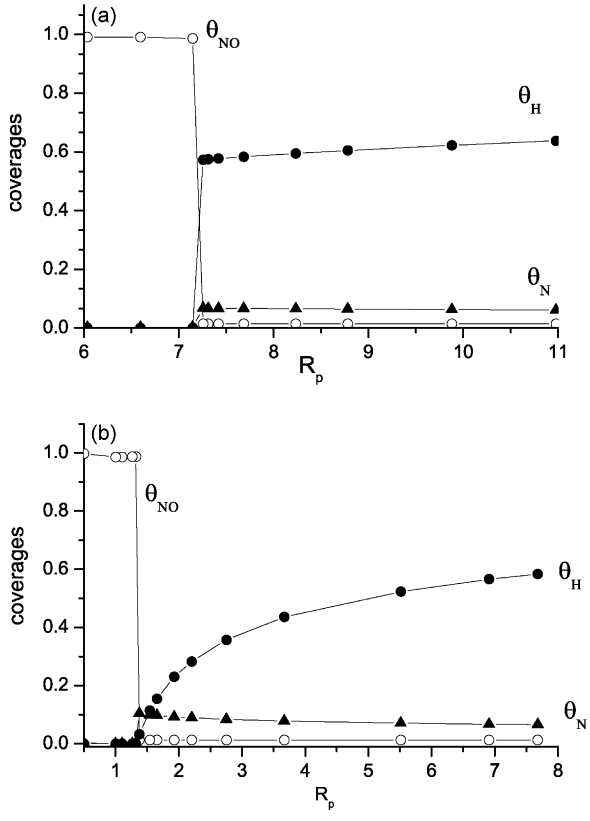

Fig. 5. Steady state coverages as a function of partial pressures R_p, same conditions in temperature and pressure as in Fig. 4. (a) Initial condition ($\theta_{NO} = 0.8, \theta_H = 0, \theta_O = 0, \theta_N = 0$); (b) initial condition ($\theta_{NO} = 0.0, \theta_H = 0, \theta_O = 0, \theta_N = 0$).

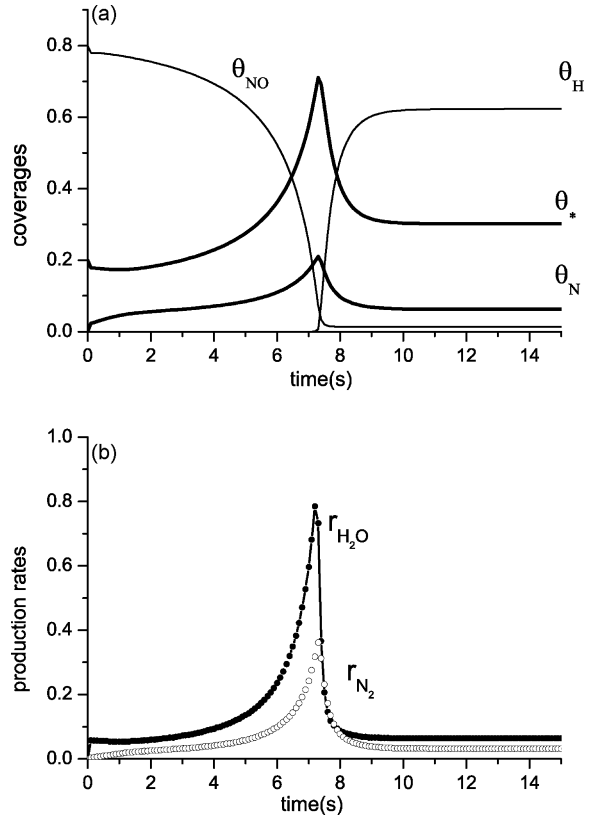

Fig. 6. Temporal evolution for an initial coverage of the species ($\theta_{NO} = 0.8, \theta_H = 0, \theta_O = 0, \theta_N = 0$), $T = 434$ K and $R_p \sim 7.5$. (a) Surface coverages and fraction of empty sites; (b) production of N_2 and H_2O.

there is a dispersion in the curves representing the production of nitrogen and water (Fig. 2b), this is because the stochasticity of the events generating the products. In fact, what it is shown in both figures is an average value from 100 trials. As more trials are averaged the curves are smoother due to lower dispersions.

The DMC simulation allows to visualize the state of dispersion of the components at different stages of the process. In Fig. 3 a–e, we show the time evolution of the species, for the time series shown in Fig. 2 a. The snapshots are shown for the time intervals indicated as arrows on the rate for N_2 ($t \sim 0, 3, 7, 10, 12, 14, 21, 39$ s). In these images, the grey dots represent adsorbed NO, black dots are adsorbed H, the green dots are adsorbed O, yellow is for adsorbed N and the white sites represent the empty sites.

The snapshots allow to visualize what happens, for example, with the production of nitrogen. Initially, the species NO and H are adsorbed randomly (Fig. 3a), after a few seconds desorption of NO takes place and empty sites appear, which allows the dissociation of NO and, consequently, oxygen and nitrogen atoms appear next to the empty sites (Fig. 3b). As can be seen from Fig. 3 c and d, this process continues on and a pattern, consisting of regions of NO surrounded by N, O and empty sites is formed. This pattern is enhanced near the peak in r_{N_2} (Fig. 3e). As the production of nitrogen decreases, the islands of NO disappear and after a long time of the process, $t \sim 39$ s (Fig. 3h), only oxygen and few nitrogen is left on the surface. So, one important result is that the species are not distributed randomly but forms

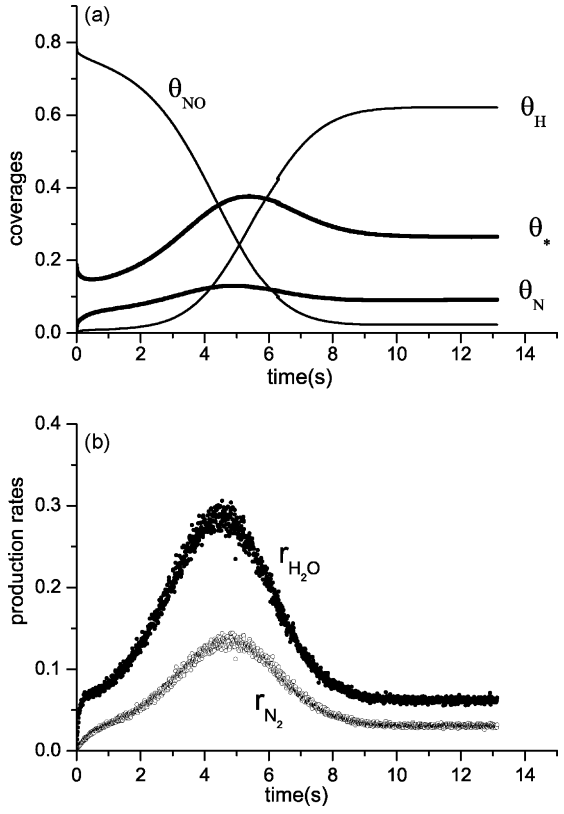

Fig. 7. DMC simulation averages over 100 trials. Temporal evolution for an initial coverage of the species ($\theta_{NO} = 0.8, \theta_H = 0, \theta_O = 0, \theta_N = 0$) and same conditions as in Fig. 6. (a) Surface coverages and fraction of empty sites; (b) production of N_2 and H_2O.

a definitive pattern. The time evolution of this pattern can be seen in the movie provided as additional material linked with this article.

We have analysed the influence of diffusion on the patterns. We basically found that diffusion acts as a stirring process. As a consequence, the patterns tend to become fuzzy at very high diffusion parameters. Our conclusion was that most of the pattern formations were essentially governed by the surface reactions. The diffusion constants that appear in partial differential equations (PDE) approach to this problem are usually macroscopic quantities, that reflects more the propagation of fronts than the true microscopic diffusion constants of the individual species. A very important parameter to take into account is the ratio δ between the rates of diffusion and the other steps, diffusion being much faster compared to the Langmuir-Hinshelwood step. In our calculations, we vary δ from 0 to about 20. It is not realistic in finite size boundary condition simulations to vary the surface diffusion coefficient D beyond a fraction of the lattice size (typically about $L/4$, where L^2 is the lattice size). Indeed, for larger values of D, the boundary conditions will allow too many particles to enter the other side of the lattice *before* any other reaction has occurred, biasing thus the correct diffusion processes. Similarly, mimicking large diffusions by random moves of the particle is also unrealistic, because the short distance correlations due to wave propagation will be lost (this argument is even more true if we imagine a much larger lattice). The only way to approach large values of D (or δ) is through larger lattice sizes. In order to reach the experimental values, our lattices must be increased by 10^4 in the best case, a value barely reachable by actual computing facilities.

3.2. Explosive behaviour in a FIM experiment

In experiments of field ion microscopy (FIM) and field electron microscopy (FEM), which are performed in a UHV (ultrahigh vacuum) chamber, an emitting tip is subjected to the $NO + H_2$ reaction. The microscope is run as a flow reactor [15–17] with a constant flux at a given temperature. The FIM images [17] show a sequence of patterns associated with a catalytic cycle associated with water formation. In order to simplify the problem we consider only the phase Pt(1 0 0) subjected to the processes described by steps $R1$–$R10$. To gain some inside about the nature of the solutions let us consider first an simplified reaction scheme given by steps $R1$–$R4$ (adsorption/desorption of NO and H_2) plus:

$$NO_{ads} + * \xrightarrow{k_{dis}} \frac{1}{2}N_2(g) + O_{ads} \quad \text{(R11)}$$

$$O_{ads} + 2H_{ads} \xrightarrow{k_r} H_2O(g) + 3* \quad \text{(R12)}$$

In this way, we consider only three species: NO, H, O.

The kinetic equations are now:

$$\frac{d\theta_{NO}(t)}{dt} = R_1 - R_3 - R_{dis} \quad (7)$$

$$\frac{d\theta_H(t)}{dt} = 2R_2 - 2R_4 - R_r \quad (8)$$

$$\frac{d\theta_O(t)}{dt} = R_{dis} - R_r \quad (9)$$

where $R_{dis} = k_{dis}\theta_{NO}\theta_*$ and $R_r = k_r\theta_O(\theta_N)^2$.

3.2.1. Stationary properties

It is possible to find analytically the stationary solutions by solving the set of Eqs. (7)–(9). In fact, from Table 1, it is seen that, for example, at $T \sim 400$ K, the rates of desorption of nitric oxide and hydrogen are, $k_3 \sim 10^{-5}$, $k_4 \sim 0.02$, respectively. Taking the limit case where the desorption of reactants is neglected, we found that the stationary solutions satisfy the equation:

$$x^3 + \left(\frac{2P_1P_2 + k_{dis}P_1 - 2k_{dis}P_2}{2k_{dis}P_2}\right)x^2 + \left(\frac{P_1^2}{2P_2K_r}\right) = 0 \quad (10)$$

$$y = \frac{P_1}{k_{dis}} \quad (11)$$

$$x + y + z + \theta_* = 1 \quad (12)$$

where $\theta_{H,est} = x$, $\theta_{NO,est} = y$, $\theta_{O,est} = z$, $P_1 = k_1 p_{NO} S_{NO}$, $P_2 = k_2 p_{H_2} S_{H_2}$

According to the theory of algebraic equations, Eq. (10) has three different real roots if the discriminant satisfies

$$\Delta = q^2 + p^3 < 0 \quad (13)$$

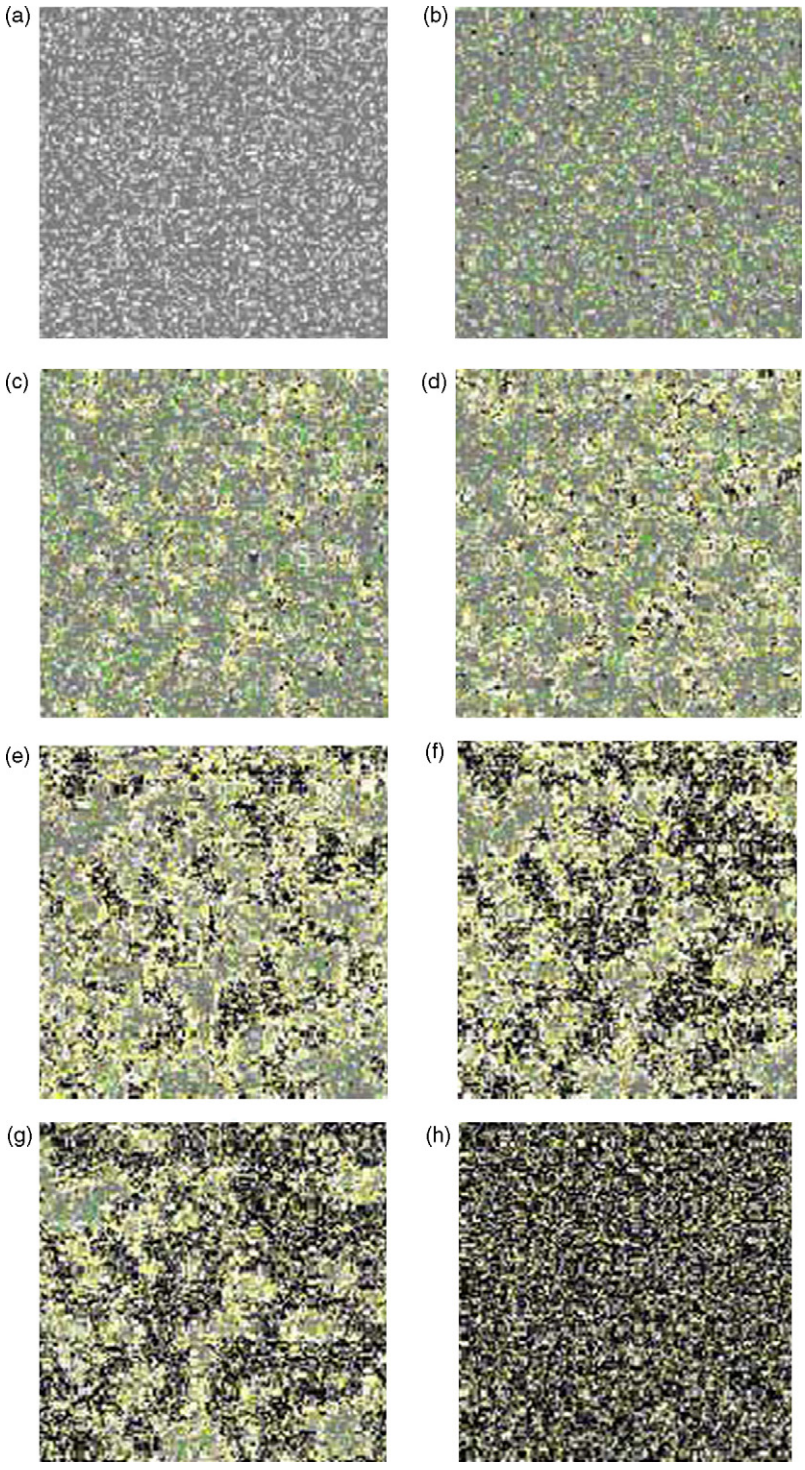

Fig. 8. (a–h) DMC simulation. The temporal evolution of the species corresponding to the time series shown in Fig. 7 b. The time increments correspond to $t = 0, 0.5, 2.5, 3, 4, 5, 6, 10$ s. In these images, the grey dots represent adsorbed NO, black dots are adsorbed H, the green dots are adsorbed O, yellow is for adsorbed N and the white sites represent the empty sites. (For interpretation of the references to colour in this figure legend, the reader is referred to the web version of the article.)

with

$$2q = \frac{2b^3}{27a^3} - \frac{bc}{3a^2} + \frac{d}{a}, 3p = \frac{3ac - b^2}{3a^2} \tag{14}$$

In the case of Eq. (10), we have

$$\Delta = \left(\frac{b^3}{27} + \frac{\mathrm{d}}{2}\right)^2 - \frac{b^6}{9^3} \tag{15}$$

Taking the values of Table 1, we have that, for example, $T \sim 400\,\mathrm{K}$, $P_1 \sim 0.2$, $P_2 \sim 1.5$, $k_{\mathrm{dis}} \sim 1$, then $y = 0.2$ and we have that condition $\Delta < 0$ is fulfilled if $k_r < 0.228$ (note that according to Table 1, $k_8 \sim 10^6$). We have then three non-trivial solutions to Eq. (10): three real roots of which two are positive. The stable solutions represent states of the surface, which are characterized by a high H concentration and low O concentration for one of them and the inverse relation for the other. For example, for $k_r \sim 10^3$, the stationary solutions are:

$$x = 0.72997,\ y = 0.2,\ z = 0.03703$$
$$x = 0.00428,\ y = 0.2,\ z = 0.76272$$

There is thus a bistability between two stable states. The same result can be obtained numerically if the above-mentioned values of k_2, k_4 are taken.

We now return to the case of four species. In a certain range of partial pressures numerical integration of the evolution Eqs. (1)–(4) confirms that there are four positive real roots and the system can exhibit bistability between different stationary states (the values of the parameters are not arbitrary but are taken from the experimental values reported in Table 1). One of the solutions is ($\theta_{\mathrm{NO}} = 0, \theta_{\mathrm{H}} = 0, \theta_{\mathrm{O}} = 1, \theta_{\mathrm{N}} = 0$), an O_{ads}-poisoned state with low reactivity coexists with a reactive low coverage state.

Fig. 4 shows the bifurcation diagram, the steady state θ_{NO} (Fig. 4a) and θ_{H} (Fig. 4b) coverages as a function of the relation of partial pressures, $R_p = P_{\mathrm{H_2}}/p_{\mathrm{NO}}$ and for $T = 434\,\mathrm{K}$. Here, $p_{\mathrm{NO}} = 1.1 \times 10^{-6}\,\mathrm{mbar}$ and $p_{\mathrm{H_2}}$ is varied. The diagram was obtained with BIFPACK (program package for continuation, bifurcation and stability analysis [25]) and is characterized by the presence of a reactive state with low $\mathrm{NO_{ads}}$ which can coexist with an inactive one, corresponding to a highly $\mathrm{NO_{ads}}$-covered state. This can be seen also in the representation of Fig. 5. Fig. 5 a corresponds to the initial condition ($\theta_{\mathrm{NO}} = 0.8, \theta_{\mathrm{H}} = 0, \theta_{\mathrm{O}} = 0, \theta_{\mathrm{N}} = 0$) and Fig. 5 b to the initial condition ($\theta_{\mathrm{NO}} = 0, \theta_{\mathrm{H}} = 0, \theta_{\mathrm{O}} = 0, \theta_{\mathrm{N}} = 0$), the reactive state with low $\mathrm{NO_{ads}}$ disappears at a critical R_p, in the first case $R_p \sim 7.31$ and in the second case $R_p \sim 1.37$.

3.2.2. Temporal behaviour

The occurrence of explosive phenomena of the $\mathrm{NO + H_2/Pt}$ reaction is associated with bistability. Indeed, around the transition point the explosive phenomena in the production of nitrogen and water is observed. As an illustration, the set of Eqs. (1)–(4) was solved for $T = 434\,\mathrm{K}$ and initial conditions ($\theta_{\mathrm{NO}} = 0.8, \theta_{\mathrm{H}} = \theta_{\mathrm{N}} = \theta_{\mathrm{O}} = 0$) at $R_p = 7.5$. In Fig. 6 a, the corresponding fraction of adsorbed species are depicted, whereas the abrupt production rate of water and nitrogen ("explosive" production) is shown in Fig. 6 b. As can be seen from both figures there are pronounced peaks in the production of both $\mathrm{H_2O}$ and $\mathrm{N_2}$ around $t \sim 7\,\mathrm{s}$. These peaks correspond well with the rapid transition from a highly NO-covered state to a less covered active surface. The dynamics is also characterized by a sudden increase in the number of empty sites, the maximum of which also occurs at around $t \sim 7\,\mathrm{s}$. The increase of empty sites is responsibly for the autocatalysis of the reaction and thus the large production of water and nitrogen.

The MC simulations also show the explosive behaviour in the production of water and nitrogen depending of the relationship between the partial pressures. For example, for the same conditions as before, Fig. 7 a shows the fraction of adsorbed species and evolution of empty sites and Fig. 7 b the sudden increase in the production of nitrogen and water. Unlike the MF case, the θ_{NO} coverage undergoes a smooth transition between its high and low coverage states. The same happens with the increase in the number of empty sites, that is, in the DMC simulation the sudden increase in water and nitrogen is less explosive.

Fig. 8 a–h shows the corresponding visualisation for the distribution of species. The snapshots were taken at $t = 0, 0.5, 2.5, 3, 4, 5, 6, 10\,\mathrm{s}$. Starting from a surface mainly covered by $\mathrm{NO_{ads}}$ ($\theta_{\mathrm{NO}} = 0.8, \theta_* = 0.2$), the NO molecules start to dissociate into N and O, the $\mathrm{N_2}$ molecules desorb and more vacant sites are created. At the same time, the adsorbed H grows and it can be observed that clusters of $\mathrm{H_{ads}}$ begin to form (black points in Fig. 8). Finally, the system attains a stationary state where $\mathrm{H_{ads}}$ and θ_* are the dominant species homogeneously distributed (Fig. 8h). The time evolution of this explosion can be seen in the movie provided as additional material linked with this article.

4. Conclusions

We have used a simplified version of the reaction $\mathrm{NO + H_2}$ on Pt(1 0 0) to simulate the phenomenon of "surface explosion" in the production of water and nitrogen observed, for example, in FEM and FIM experiments. By considering only four species, the mathematical MF model gives rise to a bistability of a highly NO-covered state and a reactive state associated to a less covered surface. By constructing the phase diagram, a sharp transition between these two sates is observed. The "surface explosion" or abrupt production of nitrogen and water is observed near the transition point.

The effects of fluctuations were also studied by DMC simulations. Including all the steps as in the mean field description, the explosive phenomena, a peak in the production of water and $\mathrm{N_2}$ is also observed. The simulations allow visualizing the distribution of adsorbed species. One important feature is the formation of adsorbed NO islands surrounded by a large quantity of empty sites, a result which is in agreement with the kinetic formulation by mean of ODE's where a maximum in the number of empty sites correlates with the nitrogen and water production, thus supporting the autocatalytic nature of the reaction. We finally want to underline that the system we have analysed here is typically in non-equilibrium state. Thus, a stochastic model of the chemical system has been built. The behaviour of the system is then determined by the rates of the reactions, which are specified as probabilities, and a Master Equation then gives the surface configuration over time. In our stochastic simulation, the rates are readily given by the experiments and the steady states are directly related to mean field formulation of the rate evolution equations. The simulations then nicely complements mean field type approach by allowing the study of the fluctuations of the surface coverage.

Moreover, the model is not able to reproduce sustained ignitions, as it is the case observed in FIM and FEM experiments. With the sole mechanism R 1–R 10, it is not possible to regenerate the catalyst and produce sustained explosions. The lacking mechanism to generate the sustained oscillations in both N_2 and H_2O production rates could be the surface transformation between hex and 1×1 phases, or, as was done in refs. [4,22] by considering more intermediate species.

Acknowledgement

Financial support from CONACYT through grant 49968 is gratefully acknowledged.

References

[1] K.C. Taylor, Automotive Catalytic Converters, Springer, Berlin, 1984.
[2] W.F. Egelhoff Jr., The Chemical physics of solid surfaces and heterogeneous catalysis, in: D.A. King, D.P. Woodruff (Eds.), Fundamental Studies of Heterogeneous Catalysis, vol. 4, Elsevier, Amsterdam, 1982.
[3] J. Siera, P. Cobden, K. Tanaka, B.E. Nieuwenhuys, Catal. Lett. 10 (1991) 335.
[4] A.G. Makeev, B.E. Nieuwenhuys, J. Chem. Phys. 108 (1998) 3740.
[5] A.G. Makeev, B.E. Nieuwenhuys, Surf. Sci. 418 (1998) 432.
[6] M.F.H. van Tol, A. Gielbert, B.E. Nieuwenhuys, Catal. Let. 16 (1992) 297.
[7] H.H. Madden, R. Imbihl, Appl. Surf. Sci. 48/49 (1991) 130.
[8] M. Slinko, T. Fink, T. Lher, H.H. Madden, S.J. Lombardo, R. Imbihl, G. Ertl, Surf. Sci. 264 (1992) 157.
[9] P.D. Cobden, J. Siera, B.E. Nieuwenhuys, J. Vac. Sci. Technol. A 10 (1992) 2487.
[10] S.J. Lombardo, Th. Fink, R. Imbihl, J. Chem. Phys. 98 (1993) 5526.
[11] M. Gruyters, A.T. Pasteur, D.A. King, J. Chem. Soc. Faraday Trans. 92 (1996) 2941.
[12] R. Imbihl, G. Ertl, Chem. Rev. 95 (1995) 697.
[13] M.M. Slinko, N.I. Jaeger, Oscillating Heterogeneous Catalytic Systems, Elsevier, Amsterdam, 1994.
[14] M.W. Lesley, L.D. Schmidt, Surf. Sci. 155 (1985) 215.
[15] C. Voss, N. Kruse, Appl. Surf. Sci. 87/88 (1994) 127.
[16] V.V. Gorodetskii, V.I. Elokhin, J.W. Bakker, B.E. Nieuwenhuys, Catal. Today 105 (2005) 183.
[17] Y. De Decker, F. Baras, N. Kruse, G. Nicolis, J. Chem. Phys. 117 (2002) 10244.
[18] R.M. Ziff, E. Gulari, Y. Barshad, Phys. Rev. Lett. 56 (1986) 2553.
[19] E.V. Albano, M. Borwko, in: Computational Methods in Surface and Colloid Science, Marcel Dekker, New York, 2000.
[20] V.P. Zhdanov, Surf. Sci. 45 (2002) 231.
[21] G. Nicolis, Faraday Discuss. 120 (2001) 1.
[22] F.V. Caballero, L. Vicente, Chem. Eng. J. 106 (2005) 229.
[23] F. Chávez, L. Vicente, A. Perera, J. Chem. Phys. 113 (2000) 10353.
[24] A. Danielak, A. Perera, M. Moreau, R. Kapral, Physica A 229 (1996) 428.
[25] R. Seydel, Practical Bifurcation and Stability Analysis, Springer, New York, 1994.